GEOLOGY | THE GEOLOGICAL SOCIETY OF AMERICA®

https://doi.org/10.1130/G51507.1

Manuscript received 27 June 2023
Revised manuscript received 27 September 2023
Manuscript accepted 25 October 2023

Published online 16 November 2023

Origin of Archean Pb isotope variability through open-system Paleoarchean crustal anatexis

M.I.H. Hartnady[1,*], C.L. Kirkand[1], S.P. Johnson[2], R.H. Smithies[1,2], L.S. Doucet[3,4], and D.R. Mole[5]

[1]Timescales of Mineral Systems Group, School of Earth and Planetary Science, Curtin University, Perth, WA 6845, Australia
[2]Geological Survey of Western Australia, 100 Plain Street, East Perth, WA 6004, Australia
[3]Earth Dynamics Research Group, School of Earth and Planetary Science, Curtin University, Perth, WA 6102, Australia
[4]State Key Laboratory of Geological Processes and Mineral Resources, China University of Geosciences, Wuhan, Hubei, 430074, China
[5]Geoscience Australia, GPO Box 378, Canberra, ACT 2601, Australia

ABSTRACT

Lead isotopic data imply that thorium and uranium were fractionated from one another in Earth's early history; however, the origin of this fractionation is poorly understood. We report new *in situ* Pb isotope data from orthoclase in 144 granites sampled across the Archean Yilgarn craton (Western Australia) to characterize its Pb isotope variability and evolution. Granite Pb isotope compositions reveal three Pb sources, a mantle-derived Pb reservoir and two crustal Pb reservoirs, distinguished by their implied source $^{232}Th/^{238}U$ (κ_{Pb}). High-κ_{Pb} granites reflect sources with high $^{232}Th/^{238}U$ (~4.7) and are largely co-located with Eoarchean–Paleoarchean crust. The Pb isotope compositions of most granites, and those of volcanic-hosted massive sulfide (VHMS) and gold ores, define a mixing array between a mantle Pb source and a Th-rich Eoarchean–Paleoarchean source. Pb isotope modeling indicates that the high-κ_{Pb} source rocks experienced Th/U fractionation at ca. 3.3 Ga. As Th/U fractionation in the Yilgarn craton must have occurred before Earth's atmosphere was oxygenated, subaerial weathering cannot explain the apparent differences in their geochemical behavior. Instead, the high Th/U source reflects Eoarchean–Paleoarchean rocks that experienced prior high-temperature metamorphism, partial melting, and melt loss in the presence of a Th-sequestering mineral like monazite. Archean Pb isotope variability thus has its origins in open-system high-temperature metamorphic processes responsible for the differentiation and stabilization of Earth's continental crust.

INTRODUCTION

Thorium and uranium are highly incompatible trace elements that are partitioned into Earth's crust over geological time (Galer and O'nions, 1985; Allègre et al., 1986). Being two of the main heat-producing elements in the silicate Earth, understanding their partitioning between different geochemical reservoirs is important for tracking our planet's thermal evolution and internal differentiation.

Thorium has a single valence state (4+) whereas U exists in two valence states (4+ and 6+), with the highly water-soluble hexavalent species dominant under oxidized surface conditions (Zartman and Haines, 1988). Since the Great Oxidation Event (2.5–2.4 Ga), U has preferentially been recycled into the mantle, causing a progressive lowering of the Th/U ratio in the mantle and in rocks derived from it (McCulloch, 1993; Collerson and Kamber, 1999; Elliott et al., 1999; Zartman and Richardson, 2005). However, in the Archean, when Earth's atmosphere was largely devoid of oxygen, neither mantle melting, fractional crystallization, nor weathering and recycling processes could have fractionated U and Th. Hence, it is thought the geochemical behavior of these elements was identical from the surface down to the upper mantle (Liu et al., 2019). Nevertheless, some lines of evidence show that Th and U were fractionated from one another early in Earth's history. For example, variability in the $^{208}Pb/^{204}Pb$ ratios of some Archean rocks and ore minerals require an older Pb source with superchondritic $^{232}Th/^{238}U$ (Robertson and Cumming, 1968; Perring and McNaughton, 1992). However, there has been no satisfactory explanation for how Th and U were fractionated from one another this early in Earth's history.

The Yilgarn craton in Western Australia provides an ideal laboratory for investigating the origins of Archean Pb isotope variability. Large volumes of granite were emplaced within a restricted time interval (2.7–2.6 Ga), via reworking of pre-existing crust of variable age (3.8–2.7 Ga; Mole et al., 2019). As the variability in initial Pb isotope composition of granites depends on the $^{238}U/^{204}Pb$ ratio (μ) and $^{232}Th/^{238}U$ ratio (κ) of their source rocks and the duration of radioactive decay, any variability in source $^{232}Th/^{238}U$ will manifest itself in their initial Pb isotope compositions. Analyzing the initial Pb isotope composition of these granites affords the opportunity to probe the deep crustal composition and architecture, and address the origins of Pb isotope variability in ancient crust. Although many rock-forming silicate minerals have non-zero U/Pb ratios, meaning their Pb isotope compositions change over time, one mineral that can yield initial Pb isotope ratios is orthoclase (Gancarz and Wasserburg, 1977).

We report new orthoclase laser ablation–inductively coupled plasma–mass spectrometry Pb isotope data from 144 samples of granite feldspar from across the Yilgarn craton. A detailed method description and data tables are provided in the Supplemental Material[1].

M.I.H. Hartnady https://orcid.org/0000-0001-5297-9925
*michael.hartnady@curtin.edu.au

[1]Supplemental Material. Analytical details and Pb isotope data tables. Please visit https://doi.org/10.1130/GEOL.S.24451885 to access the supplemental material; contact editing@geosociety.org with any questions.

CITATION: Hartnady, M.I.H., et al., 2024, Origin of Archean Pb isotope variability through open-system Paleoarchean crustal anatexis: Geology, v. 52, p. 77–81, https://doi.org/10.1130/G51507.1

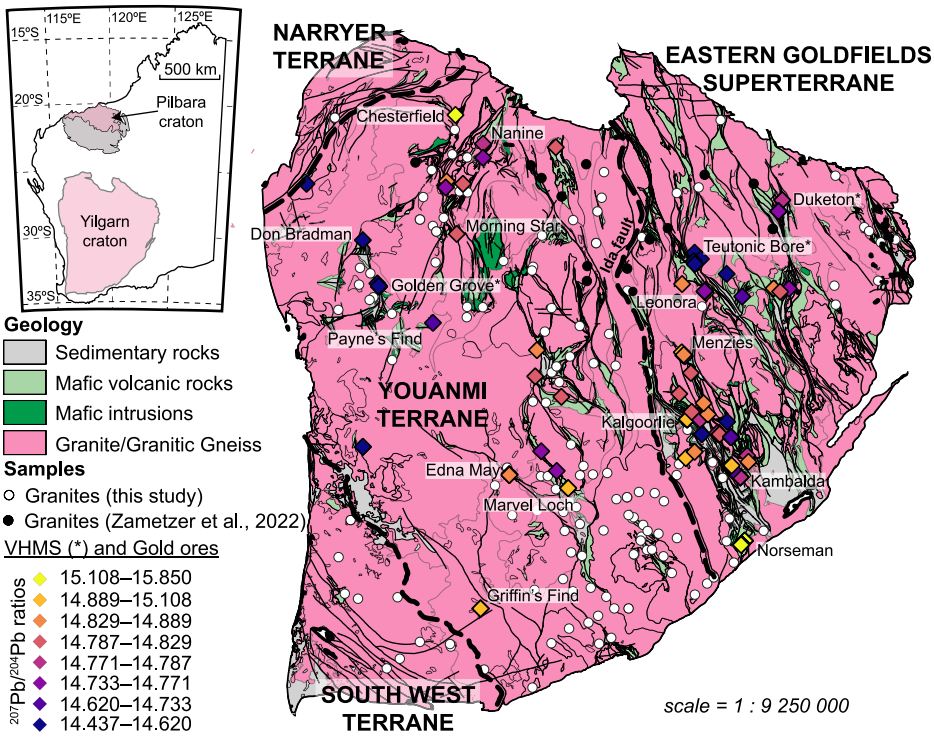

Figure 1. Map of the Yilgarn craton (Western Australia) showing the locations of important gold deposits, volcanic-hosted massive sulfide (VHMS) deposits, and granites for which Pb isotope data are available.

GEOLOGICAL SETTING

The Yilgarn craton comprises several terranes (Fig. 1). The Narryer terrane occupies the northwest corner of the craton and contains felsic gneisses with protolith ages from 3.73 Ga to 3.37 Ga, and subordinate supracrustal belts (Kinny et al., 1988; Kemp et al., 2018). Together with the South West and Youanmi terranes, they make up the West Yilgarn, which contains evidence for shared 3.00–2.90, 2.80, and 2.73–2.72 Ga magmatism generally characterized by unradiogenic Nd and Hf isotope compositions, indicating an older Paleoarchean source for this region (Mole et al., 2019). The West Yilgarn abuts the Eastern Goldfields Superterrane (EGST) along the Ida fault (Fig. 1). The EGST is dominated by felsic igneous rocks and supracrustal sequences (greenstone belts) formed between 2.72 and 2.66 Ga, representing a period of widespread basalt-komatiite magmatism, which was followed by craton-wide emplacement of tonalite-trondjhemite-granodiorite (TTG) and subsequently K-rich granite, inferred to reflect a widespread lower-crustal melting event (Smithies et al., 2019).

Pb ISOTOPE SYSTEMATICS OF THE YILGARN CRATON

Figure 2 shows the Pb isotope ratios of the granite samples along with a compilation of data from volcanic-hosted massive sulfide (VHMS) and Au ores from across the craton, and the terrestrial Pb isotope evolution model of Maltese and Mezger (2020). The range of Pb isotope compositions from the granites is identical to those of the ores (Fig. 2A and 2B), which are both consistent with modeled single-stage paleogeochrons for rocks formed between 2.7 and 2.6 Ga (Figs. 2A and 2C; Table DR1 in the Supplemental Material). The least-radiogenic granites have Pb isotope compositions approaching those of the VHMS ores at Teutonic Bore, which may approximate mantle Pb isotope compositions at that time (Hannington et al., 2005). More than 50% of the samples overlap the initial Pb isotope compositions of Au deposits from the Wiluna-Leonora and Menzies-Kambalda regions, whereas the most-radiogenic samples scatter to higher $^{206}Pb/^{204}Pb$ and $^{207}Pb/^{204}Pb$ ratios, like those associated with the Stennet Rocks granite and Au ores from the Norseman area (Figs. 2A and 2C).

The spatial variation of granite Pb isotope source model ages using interpolated isotopic maps shows a long-wavelength structure like that observed in zircon initial Hf and whole-rock initial Nd isotopes (Figs. 3A–3C). Specifically, the Youanmi terrane exhibits higher $^{206}Pb/^{204}Pb$ and $^{207}Pb/^{204}Pb$ ratios (older source model ages) and Hf model ages as old as 3.8–3.6 Ga (Fig. 3A), indicating granites in these regions sampled old felsic crust with sub-chondritic $^{176}Lu/^{177}Hf$ and $^{147}Sm/^{144}Nd$ ratios and μ higher than the bulk Earth model. Across the Ida fault, there is a gradient in both Hf model ages and granite $^{207}Pb/^{204}Pb$ source ages (Figs. 3A–3C). The EGST granites exhibit less-radiogenic Pb isotope compositions and younger Hf model ages (<2.9 Ga), indicating magmatism in the EGST was derived from source rocks with a greater amount of mantle-derived material. All the isotopic data sets are broadly consistent with the upper mantle velocity structure, which implies a density (and hence age) gradient in subcratonic lithospheric mantle (Fig. 3D; Kennett et al., 2013).

Whereas variable $^{206}Pb/^{204}Pb$ and $^{207}Pb/^{204}Pb$ ratios reflect mixing between sources with different $^{238}U/^{204}Pb$ fractionation histories, variation in $^{208}Pb/^{204}Pb$ ratios reveals sources with different $^{232}Th/^{238}U$ fractionation histories. A plot of $^{208}Pb/^{204}Pb$ versus $^{206}Pb/^{204}Pb$ reveals the high-μ crustal source comprises two separate components with distinct $^{208}Pb/^{204}Pb$ ratios. One component is defined by $^{208}Pb/^{204}Pb$ ratios >~33.7, implying an old crustal source with κ_{Pb} greater than coeval mantle (~4.75, crustal Pb source 1 in Figure 2D). A second component, defined by the Norseman gold ores, has $^{208}Pb/^{204}Pb$ ratios close to the bulk silicate Earth (BSE), implying a κ_{Pb} close to coeval mantle (~4.0, crustal Pb source 2 in Figure 2D). The scatter of most granites and ores in $^{208}Pb/^{204}Pb$ versus $^{206}Pb/^{204}Pb$ space delineates an array between a mantle Pb source and a high-μ, high-κ_{Pb} crustal source. Although mixing with the Norseman source is not well resolved by the granite data, the presence of highly radiogenic crust in this region is clear in the isotopic map.

We estimate crustal $^{238}U/^{204}Pb$, $^{232}Th/^{204}Pb$, and $^{232}Th/^{238}U$ using a two-stage Pb isotope evolution model that allows for variable mantle and crustal residence times (Delavault et al., 2016) whereby the ratios are calculated based on the evolution of Pb isotopes in the period between the zircon Hf model age and the crystallization of the granite:

$$\mu_C = \frac{\left(\frac{^{206}Pb}{^{204}Pb}\right)_{T_C} - \left(\frac{^{206}Pb}{^{204}Pb}\right)_{T_S}^{mantle}}{\left(e^{\lambda_{238}T_C} - e^{\lambda_{238}T_S}\right)}, \quad (1)$$

or

$$\mu_C = 137.88 \times \frac{\left(\frac{^{207}Pb}{^{204}Pb}\right)_{T_C} - \left(\frac{^{207}Pb}{^{204}Pb}\right)_{T_S}^{mantle}}{\left(e^{\lambda_{235}T_C} - e^{\lambda_{235}T_S}\right)}, \quad (2)$$

and

$$\Omega_C = \frac{\left(\frac{^{208}Pb}{^{204}Pb}\right)_{T_C} - \left(\frac{^{208}Pb}{^{204}Pb}\right)_{T_S}^{mantle}}{\left(e^{\lambda_{232}T_C} - e^{\lambda_{232}T_S}\right)}. \quad (3)$$

In this form, it is clear that the values of μ_c and Ω_c equate to the slope of a straight line connecting the measured initial $^{x}Pb/^{204}Pb$ ratio

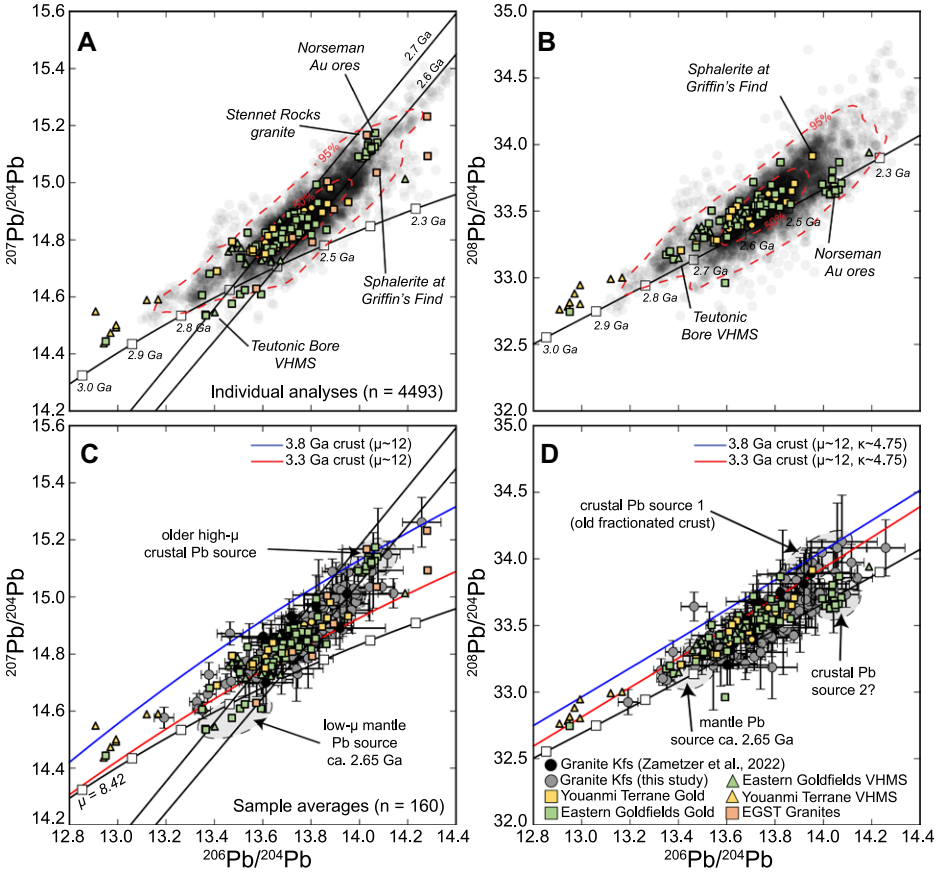

Figure 2. Pb isotope evolution diagrams showing individual orthoclase analyses (A and B) and mean and standard deviations for each granite (C and D). Growth curves and paleogeochrons are after Maltese and Mezger (2020). Red and blue curves show crustal Pb isotope evolution models for 3.8 Ga and 3.3 Ga crust, respectively. Yilgarn craton locations are shown in Figure 1. See the Supplemental Material (see text footnote 1) for details of the Pb isotope modeling. Kfs—K-feldspar; VHMS—volcanic-hosted massive sulfide; EGST—Eastern Goldfields Superterrane.

at the time of crystallization (T_c) to the mantle reference curve at the time of crust formation (T_s) in a plot of $^{x}Pb/^{204}Pb$ versus $e^{\lambda T}$, where e is Euler's constant and λ is the relevant decay constant (Figs. 3E–3G). Crust formation ages were obtained from zircon Hf isotope compositions (Mole et al., 2019) re-calculated using the measured Hf isotope ratios, the ^{176}Lu decay constant of Söderlund et al. (2004), and the depleted mantle parameters of Griffin et al. (2000). Mantle Pb isotope evolution is modeled using the single stage model, after Maltese and Mezger (2020), with $\mu = 8.42$ and $\kappa = 4.03$. Using this approach, we calculate an average crustal $^{238}U/^{204}Pb$ of 11.3 ± 2.1 and $^{232}Th/^{204}Pb$ of 47.4 ± 10.0, which equates to a $^{232}Th/^{238}U$ of 4.2 ± 0.3 (Figs. 3E–3G and 4)

ORIGIN OF ARCHEAN Pb ISOTOPE VARIABILITY

Recent estimates of crustal $^{232}Th/^{238}U$ based on a global data set of continental rocks yielded a median value of 3.95 (Wipperfurth et al., 2018). The similarity with modern mantle and primordial $^{232}Th/^{238}U$ ratios led that study to conclude negligible fractionation of Th and U during either segregation of Earth's core following accretion, or during crust extraction out of the mantle. Although our results overlap previous estimates for the continental crust, we obtain a crustal κ_{Pb} ~10% higher than estimates for the bulk silicate Earth on average (Fig. 4). The Yilgarn granite and ore Pb isotope data scatter between a mantle component, defined by some VHMS ores, and a more-radiogenic crustal reservoir. Therefore, the higher average κ_{Pb} of Archean crust is unlikely to reflect higher mantle Th/U ratios at that time, but rather reflects mixing between a broadly chondritic mantle reservoir and a preexisting Paleoarchean crustal Pb reservoir with $^{232}Th/^{238}U$ of ~4.7–4.8, requiring ~25% enrichment in Th relative to bulk Earth.

The presence of a high-Th/U crustal reservoir demonstrates that fractionation of Th and U accompanied early crust formation and differentiation. As Earth's atmosphere was devoid of oxygen at this time, both Th and U existed in their 4+ valence state, with any difference in partitioning during mantle melting expressed only at low degrees of partial melting. The presence of ultramafic volcanic rocks (i.e., komatiite) and higher abundance of high-Mg basalts in greenstone belts throughout the Yilgarn craton indicates Earth's mantle was warmer, and degrees of partial melting were generally higher, than today (Herzberg et al., 2010). Hence, fractionation of Th and U during extraction of crust from the early Archean mantle is unlikely to account for the difference in Pb isotope variability of Archean crust. Geochemical data from modern arc lavas imply that magmatic differentiation processes do not significantly fractionate Th and U (Liu et al., 2019). The apparent Th/U variability of early Archean crust must therefore reflect some other processes that occurred after crust formation. The granites with the highest $^{208}Pb/^{204}Pb$ ratios predominantly occur within the older western Yilgarn craton and are concentrated in regions with Paleoarchean Hf and Nd model ages (Fig. 2). A spatial analysis of the whole-rock geochemical data from the Yilgarn craton also indicates that one specific variety of potassic granite—the low-Ca, high Ti granites—are high-temperature granites concentrated in regions with old model ages. Both observations suggest that many of the granites in these parts of the craton formed by high-temperature partial melting of old refractory felsic source rocks (Smithies et al., 2023).

Th and U may be fractionated during open-system high-temperature metamorphism (Yakymchuk and Brown, 2019). In supra-solidus crust, the distribution of Th and U between a partial melt and the residual solids is strongly influenced by the breakdown and (re)growth of accessory minerals (e.g., zircon, monazite, and apatite; Yakymchuk and Brown, 2019). When present, monazite is most influential, owing to its strong preference for Th over U, although this can vary with melt composition and the behavior of coexisting apatite (Xing et al., 2013; Yakymchuk, 2017). Eoarchean–Paleoarchean granulites exposed in the Narryer terrane in the northwestern parts of the Yilgarn craton underwent partial melting involving zircon and monazite (re)growth as early as 3.3 Ga (Kinny et al., 1988; Iizuka et al., 2010). Thus, the Yilgarn Pb isotope variability can be explained either by re-melting residual Eoarchean–Paleoarchean crust or bulk assimilation/hybridization of mantle-derived melts with this material. Both processes may have occurred during lithospheric thinning and/or underplating associated with Neoarchean basalt-komatiite volcanism.

A caveat here is monazite usually grows in low-Ca peraluminous rocks, which are not major components of Archean terranes (Moyen and Laurent, 2018). In mafic systems, which may better reflect early Archean crust, the partitioning of Th and U between melt and rutile could also form high-Th/U melts (Fig. 4B; Klemme et al., 2005; Emo et al., 2023). Although the generation of the high-Th/U signature via earlier melting and/or crystal fractionation processes involving rutile cannot be *a priori* excluded, a paucity of mafic material in the Narryer terrane (Kemp et al., 2018), and dominance of low-Ca

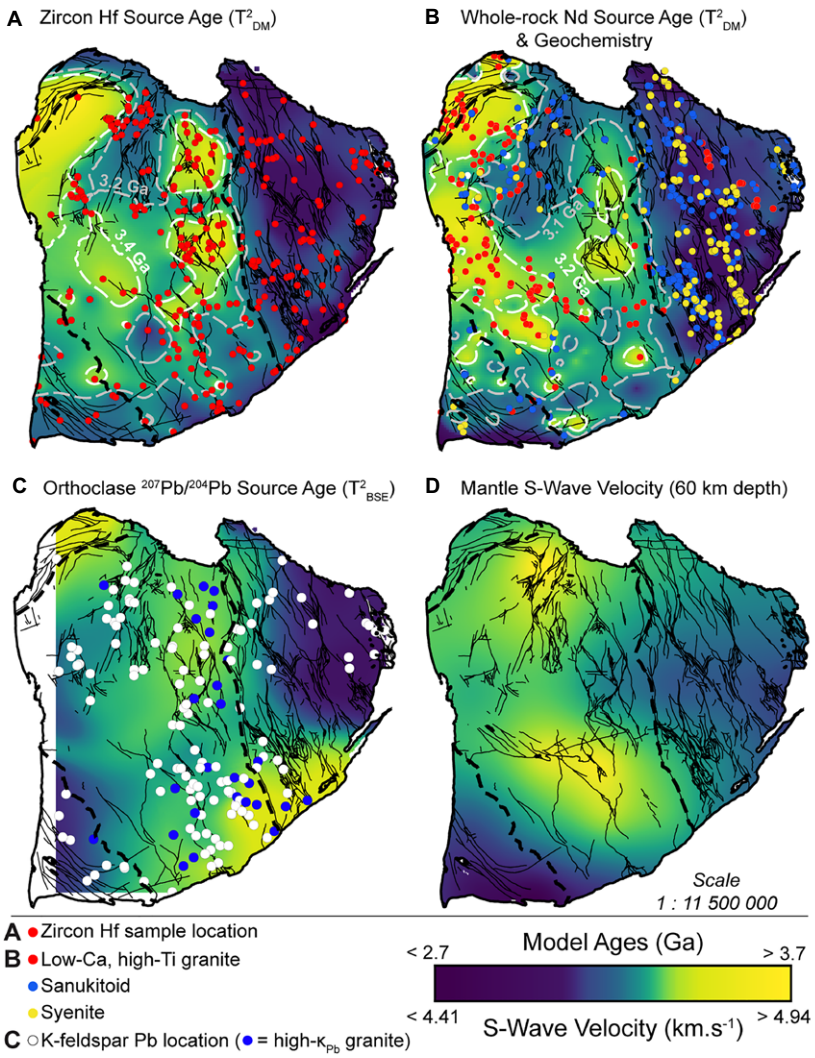

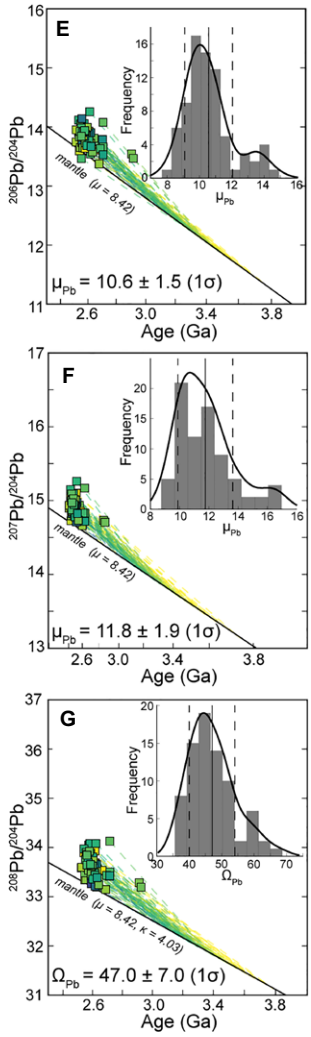

Figure 3. Maps of zircon Hf model ages (A), whole rock Nd models ages (based on regional databases from the Geological Survey of Western Australia, with samples color-coded according to the whole-rock geochemistry classification of Smithies et al. [2023]) (B), and two-stage $^{207}Pb/^{204}Pb$ source ages of granites (C), along with upper-mantle S-wave velocity from the AuSREM model (http://rses.anu.edu.au/seismology/AuSREM/index.php) from the Yilgarn craton (Kennett et al., 2013) (D). Regional variations in granite Pb isotope composition mimic Hf (and Nd) maps and mantle velocity structure indicating crust age exerts a first-order control on long-wavelength Pb isotope variability. (E–G) Pb isotope composition versus $e\lambda^t$, where e is Euler's constant and λ and is the relevant decay constant (after Albarede and Juteau, 1984) and inset histograms illustrating the calculation and distribution of two-stage crustal μ_{Pb} and Ω_{Pb} values. μ—$^{238}U/^{204}Pb$; Ω—$^{232}Th/^{204}Pb$; κ—$^{232}Th/^{238}U$; T^2_{DM}—two-stage depleted mantle model age; T^2_{BSE}—two-stage bulk silicate earth model age.

granites in the west Yilgarn (Smithies et al., 2023), suggests the ancient crustal nuclei were sufficiently differentiated to stabilize monazite.

If this is true, the formation of a melt-depleted high-Th/U lower crustal residue requires the loss of a complementary low-Th/U silicate melt to the mid-upper crust. However, we find little evidence of this complementary reservoir in the Yilgarn Pb isotope data set. Only a few samples yield κ_{Pb} values lower than the primordial value of 3.8 (Fig. 4A), indicating low-Th/U material was not overly abundant in the Neoarchean granite sources. Although this may be an artifact of limited sampling in Mesoarchean and Paleoarchean crust, it could also indicate much of this low-Th/U material was lost from the crustal record. Our preferred model requires erosion of U-rich upper crust to explain this. Indeed, the deposition of Mount Narryer and Jack Hills metasediments between 3.2 and 3.0 Ga (Iizuka et al., 2010; Kinny et al., 2022) indicates the basement

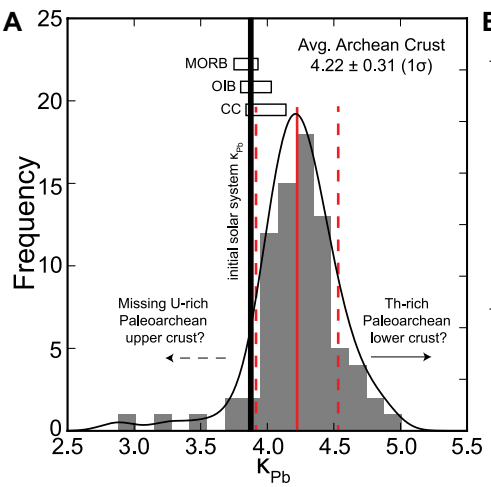

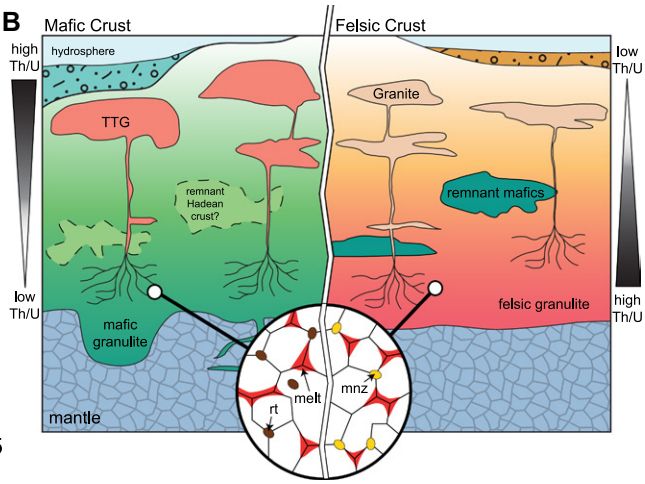

Figure 4. (A) Distribution of κ_{Pb} ($^{232}Th/^{238}U$) values relative to other silicate reservoirs. The initial solar system value is after Blichert-Toft et al. (2010); other reservoirs are after Wipperfurth et al. (2018). MORB—mid-ocean ridge basalt; OIB—ocean island basalt; CC—continental crust. (B) Schematic diagram depicting potential crustal differentiation scenarios forming the high-Th/U signature. TTG—tonalite–trondhjemite–granodiorite; rt—rutile; mnz—monazite.

gneisses were brought from suprasolidus to surface conditions during this time. However, the same outcome could occur via delamination of dense low-Th/U mafic residues formed by earlier crustal differentiation processes (Fig. 4B; Emo et al., 2023). These mechanisms are not mutually exclusive and both could have contributed to the high Th/U signature at different times in craton development. Regardless, it seems clear that the fractionation of Th and U during the early Archean was intimately linked to intra-crustal differentiation processes that stabilized Earth's continental crust, with accessory minerals playing a crucial role.

ACKNOWLEDGMENTS

This work was supported by an Australian Research Council (ARC) Linkage Project (LP180100199) in collaboration with the Geological Survey of Western Australia (GSWA) and Northern Star Resources Ltd. Insightful reviews by Tim Elliott and Balz Kamber significantly improved the manuscript. Thanks to Brian Kennett for providing the AUSREM data, to Noreen Evans, Brad McDonald, and Kai Rankenburg for analytical assistance, and to Marc Norman for editorial handling. Research at Curtin was enabled by AuScope and the Australian Government via funding from the ARC (LE150100013). SPJ and RHS publish with permission from the executive director of the GSWA. DRM publishes with permission from the CEO of Geoscience Australia.

REFERENCES CITED

Albarède, F., and Juteau, M., 1984, Unscrambling the lead model ages: Geochimica et Cosmochimica Acta, v. 48, p. 207–212, https://doi.org/10.1016/0016-7037(84)90364-8.

Allègre, C.J., Dupré, B., and Lewin, E., 1986, Thorium/uranium ratio of the Earth: Chemical Geology, v. 56, p. 219–227, https://doi.org/10.1016/0009-2541(86)90005-7.

Blichert-Toft, J., Zanda, B., Ebel, D.S., and Albarède, F., 2010, The solar system primordial lead: Earth and Planetary Science Letters, v. 300, p. 152–163, https://doi.org/10.1016/j.epsl.2010.10.001.

Collerson, K.D., and Kamber, B.S., 1999, Evolution of the continents and the atmosphere inferred from Th-U-Nb systematics of the depleted mantle: Science, v. 283, p. 1519–1522, https://doi.org/10.1126/science.283.5407.1519.

Delavault, H., Dhuime, B., Hawkesworth, C.J., Cawood, P.A., Marschall, H., and the Edinburgh Ion Microprobe Facility, 2016, Tectonic settings of continental crust formation: Insights from Pb isotopes in feldspar inclusions in zircon: Geology, v. 44, p. 819–822, https://doi.org/10.1130/G38117.1.

Elliott, T., Zindler, A., and Bourdon, B., 1999, Exploring the kappa conundrum: The role of recycling in the lead isotope evolution of the mantle: Earth and Planetary Science Letters, v. 169, p. 129–145, https://doi.org/10.1016/S0012-821X(99)00077-1.

Emo, R.B., Kamber, B.S., Downes, H., Murphy, D.T., and Caulfield, J.T., 2023, A new compositional estimate for refractory lower continental crust with implications for the first terrestrial Pb-isotope paradox. Lithos, v. 436, https://doi.org/10.1016/j.lithos.2022.106976.

Galer, S.J.G., and O'Nions, R.K., 1985, Residence time of thorium, uranium and lead in the mantle with implications for mantle convection: Nature, v. 316, p. 778–782, https://doi.org/10.1038/316778a0.

Gancarz, A.J., and Wasserburg, G.J., 1977, Initial Pb of the Amîtsoq gneiss, West Greenland, and implications for the age of the Earth: Geochimica et Cosmochimica Acta, v. 41, p. 1283–1301, https://doi.org/10.1016/0016-7037(77)90073-4.

Griffin, W.L., Pearson, N.J., Belousova, E., Jackson, S.V., van Achterbergh, E., O'Reilly, S.Y., and Shee, S.R., 2000, The Hf isotope composition of cratonic mantle: LAM-MC-ICPMS analysis of zircon megacrysts in kimberlites: Geochimica et Cosmochimica Acta, v. 64, p. 133–147, https://doi.org/10.1016/S0016-7037(99)00343-9.

Hannington, M.D., De Ronde, C.E., and Petersen, S., 2005, Sea-floor tectonics and submarine hydrothermal systems, *in* Hedenquist, J.W., et al., eds., Economic Geology, One Hundredth Anniversary Volume: p. 111–141, https://doi.org/10.5382/AV100.06.

Herzberg, C., Condie, K., and Korenaga, J., 2010, Thermal history of the Earth and its petrological expression: Earth and Planetary Science Letters, v. 292, p. 79–88, https://doi.org/10.1016/j.epsl.2010.01.022.

Iizuka, T., McCulloch, M.T., Komiya, T., Shibuya, T., Ohta, K., Ozawa, H., Sugimura, E., and Collerson, K.D., 2010, Monazite geochronology and geochemistry of meta-sediments in the Narryer Gneiss Complex, Western Australia: Constraints on the tectonothermal history and provenance: Contributions to Mineralogy and Petrology, v. 160, p. 803–823, https://doi.org/10.1007/s00410-010-0508-0.

Kemp, A., Wilde, S., and Spaggiari, C., 2018, The Narryer Terrane, Yilgarn Craton, Western Australia: A Review, *in* van Kranendonk, M.J., et al., eds., Earth's Oldest Rocks: Amsterdam, Elsevier, p. 401–433, https://doi.org/10.1016/S0166-2635(07)15036-2.

Kennett, B.L., Fichtner, A., Fishwick, S., and Yoshizawa, K., 2013, Australian seismological reference model (AuSREM): Mantle component: Geophysical Journal International, v. 192, p. 871–887, https://doi.org/10.1093/gji/ggs065.

Kinny, P.D., Williams, I., Froude, D., Ireland, T., and Compston, W., 1988, Early Archaean zircon ages from orthogneisses and anorthosites at Mount Narryer, Western Australia: Precambrian Research, v. 38, p. 325–341, https://doi.org/10.1016/0301-9268(88)90031-9.

Kinny, P.D., Clark, C., Kirkland, C.L., Hartnady, M., Gillespie, J., Johnson, T.E., and McDonald, B., 2022, How old are the Jack Hills metasediments really?: The case for contamination of bedrock by zircon grains in transported regolith: Geology, v. 50, p. 721–725, https://doi.org/10.1130/G49822.1.

Klemme, S., Prowatke, S., Hametner, K., and Günther, D., 2005, Partitioning of trace elements between rutile and silicate melts: Implications for subduction zones: Geochimica et Cosmochimica Acta, v. 69, p. 2361–2371, https://doi.org/10.1016/j.gca.2004.11.015.

Liu, H., Zartman, R.E., Ireland, T.R., and Sun, W.D., 2019, Global atmospheric oxygen variations recorded by Th/U systematics of igneous rocks: Proceedings of the National Academy of Sciences of the United States of America, v. 116, p. 18,854–18,859, https://doi.org/10.1073/pnas.1902833116.

Maltese, A., and Mezger, K., 2020, The Pb isotope evolution of Bulk Silicate Earth: Constraints from its accretion and early differentiation history: Geochimica et Cosmochimica Acta, v. 271, p. 179–193, https://doi.org/10.1016/j.gca.2019.12.021.

McCulloch, M.T., 1993, The role of subducted slabs in an evolving earth: Earth and Planetary Science Letters, v. 115, p. 89–100, https://doi.org/10.1016/0012-821X(93)90215-U.

Mole, D., Kirkland, C., Fiorentini, M., Barnes, S., Cassidy, K., Issac, C., Belousova, E., Hartnady, M., and Thebaud, N., 2019, Time-space evolution of an Archean craton: A Hf-isotope window into continent formation: Earth-Science Reviews, v. 196, 102831, https://doi.org/10.1016/j.earscirev.2019.04.003.

Moyen, J.F., and Laurent, O., 2018, Archaean tectonic systems: A view from igneous rocks: Lithos, v. 302–303, p. 99–125, https://doi.org/10.1016/j.lithos.2017.11.038.

Perring, C.S., and McNaughton, N.J., 1992, The relationship between Archaean gold mineralization and spatially associated minor intrusions at the Kambalda and Norseman gold camps, Western Australia: Lead isotope evidence: Mineralium Deposita, v. 27, p. 10–22, https://doi.org/10.1007/BF00196076.

Robertson, D.K., and Cumming, G.L., 1968, Lead- and sulfur-isotope ratios from the Great Slave Lake area, Canada: Canadian Journal of Earth Sciences, v. 5, p. 1269–1276, https://doi.org/10.1139/e68-125.

Smithies, R.H., et al., 2019, No evidence for high-pressure melting of Earth's crust in the Archean: Nature Communications, v. 10, 5559, https://doi.org/10.1038/s41467-019-13547-x.

Smithies, R.H., Lowrey, J.R., Champion, D.C., Lu, Y., and Gessner, K., 2023, Spatial trends and relationships emerging from the systematic classification of granitic rocks of the Yilgarn Craton: East Perth, Australia, Geological Survey of Western Australia, Record 2023/5, 33 p., https://nla.gov.au/nla.obj-3196299923/view.

Söderlund, U., Patchett, P.J., Vervoort, J.D., and Isachsen, C.E., 2004, The ^{176}Lu decay constant determined by Lu–Hf and U–Pb isotope systematics of Precambrian mafic intrusions: Earth and Planetary Science Letters, v. 219, p. 311–324, https://doi.org/10.1016/S0012-821X(04)00012-3.

Wipperfurth, S.A., Guo, M., Šrámek, O., and McDonough, W.F., 2018, Earth's chondritic Th/U: Negligible fractionation during accretion, core formation, and crust–mantle differentiation: Earth and Planetary Science Letters, v. 498, p. 196–202, https://doi.org/10.1016/j.epsl.2018.06.029.

Xing, L., Trail, D., and Watson, E.B., 2013, Th and U partitioning between monazite and felsic melt: Chemical Geology, v. 358, p. 46–53, https://doi.org/10.1016/j.chemgeo.2013.07.009.

Yakymchuk, C., 2017, Behaviour of apatite during partial melting of metapelites and consequences for prograde suprasolidus monazite growth: Lithos, v. 274–275, p. 412–426, https://doi.org/10.1016/j.lithos.2017.01.009.

Yakymchuk, C., and Brown, M., 2019, Divergent behaviour of Th and U during anatexis: Implications for the thermal evolution of orogenic crust: Journal of Metamorphic Geology, v. 37, p. 899–916, https://doi.org/10.1111/jmg.12469.

Zametzer, A., Kirkland, C.L., Hartnady, M.I.H., Barham, M., Champion, D.C., Bodorkos, S., Smithies, R.H., and Johnson, S.P., 2022, Applications of Pb isotopes in granite K-feldspar and Pb evolution in the Yilgarn Craton: Geochimica et Cosmochimica Acta, v. 320, p. 279–303, https://doi.org/10.1016/j.gca.2021.11.029.

Zartman, R.E., and Haines, S.M., 1988, The plumbotectonic model for Pb isotopic systematics among major terrestrial reservoirs—A case for bi-directional transport: Geochimica et Cosmochimica Acta, v. 52, p. 1327–1339, https://doi.org/10.1016/0016-7037(88)90204-9.

Zartman, R.E., and Richardson, S.H., 2005, Evidence from kimberlitic zircon for a decreasing mantle Th/U since the Archean: Chemical Geology, v. 220, p. 263–283, https://doi.org/10.1016/j.chemgeo.2005.04.003.

Printed in the USA